ORIGINAL PAPER

LaNi$_{0.5}$Ti$_{0.5}$O$_3$/CoFe$_2$O$_4$-based sensor for sensitive determination of paracetamol

Daixin Ye · Yanhong Xu · Liqiang Luo · Yaping Ding ·
Yulong Wang · Xiaojuan Liu

Abstract A novel electrochemical sensor based on LaNi$_{0.5}$Ti$_{0.5}$O$_3$/CoFe$_2$O$_4$ nanoparticle-modified electrode (LNT–CFO/GCE) for sensitive determination of paracetamol (PAR) was presented. Experimental conditions such as the concentration of LNT–CFO, pH value, and applied potential were investigated. Under the optimum conditions, the electrochemical performances of LNT–CFO/GCE have been researched on the oxidation of PAR. The electrochemical behaviors of PAR on LNT–CFO/GCE were investigated by cyclic voltammetry. The results showed that LNT–CFO/GCE exhibited excellent promotion to the oxidation of PAR. The over-potential of PAR decreased significantly on the modified electrode compared with that on bare GCE. Furthermore, the sensor exhibits good reproducibility, stability, and selectivity in PAR determination. Linear response was obtained in the range of 0.5 to 901 μM with a detection limit of 0.19 μM for PAR.

Keywords LaNi$_{0.5}$Ti$_{0.5}$O$_3$/CoFe$_2$O$_4$ · Perovskite-type nanoparticles · Paracetamol · Electrooxidation

D. Ye · L. Luo · Y. Ding (✉) · Y. Wang · X. Liu
Department of Chemistry, Shanghai University,
Shanghai 200444, People's Republic of China
e-mail: wdingyp@sina.com

Y. Xu · Y. Ding
Shanghai Key Laboratory of Modern Metallurgy and Materials
Processing, School of Materials Science and Engineering,
Shanghai University,
Shanghai 200444, People's Republic of China

Introduction

At present, metal and semiconductor nanomaterials have been extensively utilized to build electrochemical biosensors. However, most of the recent promising works employ nanostructured materials for the fabrication of biosensors because nanomaterials possess high surface volume ratio and unique physical and chemical properties [1]. Many efforts have been made to date for designing novel sensing systems and enhancing the electrochemical performance of such biosensors through tailoring the component, size, structure, and shape of the nanomaterial [2]. The perovskite-type oxide is a frequently encountered structure in inorganic chemistry, and this structure can accommodate most of the metallic ions in the periodic table with a significant number of different anions. A number of properties such as photocatalytic property [3], magnetic properties [4], conductivity, and dielectric property [5–8] have been widely investigated. Being one of popular materials, perovskite-type oxide has been used in the areas of electrochemical gas sensors [9], solid fuel cells [10–14], thermoelectric materials [15, 16], and lots of oxidation and reduction catalytic processes [17]. In recent years, as a catalyst, inorganic perovskite-type nanomaterials have received more and more attention in the area of chemically modified electrode. For example, Wang et al. have reported electrocatalytic activity of La$_{1−x}$Sr$_x$MnO$_3$ towards hydrogen peroxide reduction in alkaline medium [18]. Anh et al. have studied the catalytic properties of La$_{1−x}$Sr$_x$CoO$_{3−δ}$ (x=0.5) to hydrogen peroxide [19]. A thin layer of La$_{1−x}$Sr$_x$CoO$_{3−δ}$ (x=0.5) perovskite-type oxide was deposited on a Pt electrode by using the pulsed laser deposition technique to detect hydrogen peroxide, which showed the possibility to use this perovskite-type oxide as a sensing material for potentiometric hydrogen peroxide sensors.

Paracetamol (PAR) is an effective and safe analgesic agent used to reduce fever, cough, and cold. It is also used worldwide for the relief of mild to moderate pain associated with headache, migraine headache, and noninflammatory conditions in patients prone to gastric symptoms [20]. There is also some evidence to suggest that PAR may offer some protection against ovarian cancer and shows no propensity to be addictive, even in people who use it frequently. When used in proper therapeutic dose, PAR is readily metabolized. However, overdoses of PAR produce toxic metabolite accumulation that causes acute hepatic necrosis, inducing morbidity and mortality in humans. Thus, it is very important to develop an analytical technique for the determination of PAR in pharmaceutical preparations [21–23]. Various techniques have been reported for the determination of PAR such as high-performance liquid chromatography, on-line electrochemistry/liquid chromatography/mass spectrometry [24], spectrofluorometry, spectrophotometry [25], and chemiluminescence [26]. However, many of the methods mentioned above require several time-consuming operations, sophisticated instruments, and special training. It is apparent that less cumbersome, fast, reliable, sensitive, simple, and inexpensive techniques are needed for the determination of many compounds. Electroanalytical techniques just possessing the above characteristics have been used for the determination of PAR [27, 28]. Li et al. [29] have used MWCNTs–PANIFAD biocomposite film-modified gold electrode for sensitive determination of PAR by means of cyclic voltammetry (CV). Wang et al. [30] have studied carbon-coated nickel magnetic nanoparticle-modified glassy carbon electrode (GCE) for determination of PAR by using differential pulse voltammetry. Goyal et al. [21] have reported that nanogold-modified indium tin oxide electrode was used for the determination of PAR at pH 7.2. A graphene-based electrochemical sensor has been fabricated by Kang et al. for sensitive detection of [31]. The electrochemical behaviors of PAR on graphene-modified GCE were investigated by CV and square-wave voltammetry. However, few details were reported for the determination of PAR by electrochemical sensor based on perovskite-type oxide-modified electrode.

In the present work, $LaNi_{0.5}Ti_{0.5}O_3/CoFe_2O_4$ (LNT–CFO) nanoparticle-modified GCE was fabricated. The electrochemical properties of LNT–CFO nanoparticles towards the oxidation of PAR were studied.

Experimental

Apparatus and reagents

All electrochemical measurements were carried out on a CHI 660C electrochemical workstation (Shanghai Chenhua Co. Ltd., China). A three-electrode system was used with the modified GCE, platinum wire auxiliary electrode, and a saturated calomel reference electrode. Powder X-ray diffraction (XRD) patterns were obtained on Rigaku DLMAX-2200 X-ray diffraction using Cu $K\alpha$ radiation ($\lambda = 1.5418$Å, 40 kV, 40 mA; scanning rate, $0.08°$ s^{-1}) in the range of 10–90°. Transmission electron microscopy (TEM) of LNT–CFO was obtained by a TEM (JEOL JEM-200CX working at 160 kV) instrument.

PAR was purchased from Aladdin Chemical Reagent Co., Ltd. (Shanghai, China). All reagents were of analytical reagent grade. All solutions were prepared with double-distilled water. A 0.1M phosphate buffer solution (PBS) was chosen as the supporting electrolyte. All experiments were carried out at room temperature.

Synthesis of LNT–CFO nanoparticles

CFO was synthesized according to [32]. The first step was synthesis of $Co–Fe^{2+}–Fe^{3+}$-layered double hydroxide (LDH) sulfates. Then, the synthesized $Co–Fe^{2+}–Fe^{3+}$-LDHs were calcined in air at 900 °C for 2 h at a heating rate of 10 °C/min and then the resulting products were slowly cooled to room temperature. Finally, using the conventional ceramic method and the wet chemical method, CFO was synthesized. Sol–gel method was used to synthesize a series of the perovskite and related compounds LNT and LNT–CFO according to [33].

Preparation of LNT–CFO-modified electrode

LNT–CFO nanoparticles (1 mg) were dispersed in 1 mL double-distilled water and the mixture was agitated in an ultrasonic bath for an hour to achieve a well-dispersed suspension. Prior to use, the bare GCE (i.d.=3 mm) was polished to a mirror-like surface with 0.3 and 0.05 μm α-Al_2O_3 then rinsed ultrasonically with nitric acid, absolute ethanol, and double-distilled water, respectively. To modify the GCE with LNT–NFO nanoparticles, 5 μL of LNT–NFO nanoparticle suspension was cast on the surface of the well-polished GCE and the solvent was allowed to dry under an infrared lamp for 10 min. So, the loading value should be 0.07 mg/cm^2.

Results and discussion

Characterization of the synthesized samples

The structure of LNT–NFO nanoparticles was investigated by XRD measurements and the XRD pattern is shown in Fig. 1. The characteristic reflections of the sample are shown at 2θ angles of 22.84°, 32.34°, 39.72°, 46.23°, 52.07°, 57.53°, 67.53°, 72.24°, and 78.34° corresponding to the (1 0 0), (1 1 0), (1 1 1), (2 0 0), (2 1 0), (2 1 1), (2 2 0), (2 2 1), and (3 1 0)
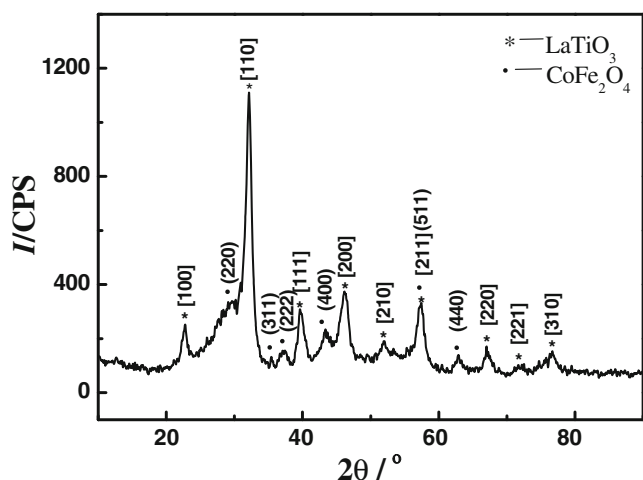
Fig. 1 XRD patterns of LNT–CFO

lattice planes, respectively, which matched well with the standard XRD pattern of LaTiO$_3$ (JCPDS file 75–0267). The calculated lattice constant is 3.913Å for LNT and 3.200Å for LaTiO$_3$. The results show that, with the doping of Ni, the lattice parameter gets smaller. It is expected that the substitution of the smaller Ni (1.25Å) for Ti (1.47Å) at the B site results in lattice shrinkage. At the same time, a collection of characteristic peaks can be observed at 2θ angles of 30.09°, 35.38°, 36.99°, 43.05°, 57.54°, and 62.75° corresponding to the (2 2 0), (3 1 1), (2 2 2), (4 0 0), (5 1 1), and (4 4 0) lattice planes, respectively, which are attributed to the structure of CoFe$_2$O$_4$ (JCPDS file 22–1086). These peaks with lower intensity due to a relatively lower content of CoFe$_2$O$_4$ suggest that the introduction of CoFe$_2$O$_4$ does not influence the structure of LNT and these two phases maintain their specific structures. The morphology of LNT-CFO nanoparticles was studied by TEM as shown in Fig. S1 of the "Electronic supplementary material". The typical TEM image of LNT-CFO NPs exhibits that the shape of these nanoparticles is close to spherical NPs. The average particle diameter is in the range of 10–30 nm.
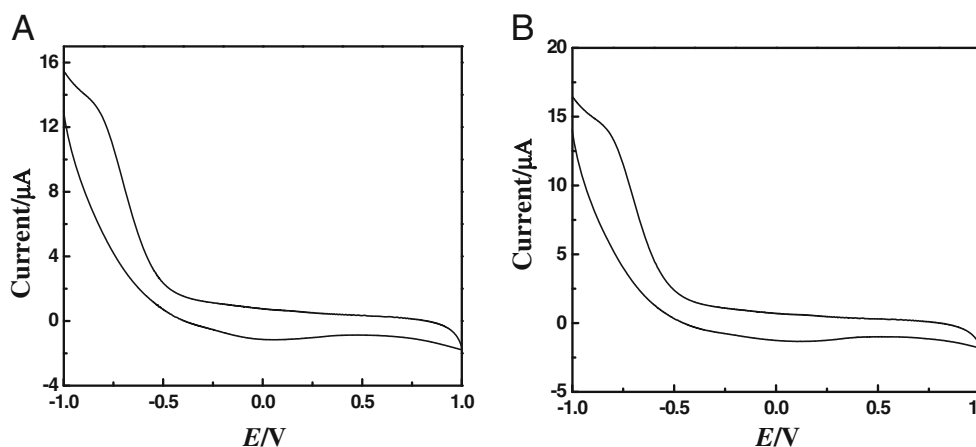
Electrochemical response of LNT–CFO/GCE to PAR

Figure 2a, b shows the CVs of bare GCE and LNT–CFO/GCE in pH 7.0 PBS. No response can be observed in the scanned potential window. After addition of PAR, CV response can be observed, as shown in Fig. 3. For the bare GCE, only a small anodic peak was observed in the potential range of −0.6–0.8 V (Fig. 3, curve b), and the E_{pa} (anodic peak potential) was +0.543 V. However, the CV curve of PAR on LNT–CFO/GCE (Fig. 3, curve a) showed a pair of redox peaks: E_{pa}=+0.467 V and E_{pc} (cathodic peak potential)=−0.019 V. Upon the addition of PAR, there is a great enhancement of the oxidation peak current compared to the bare GCE. Lower overvoltage for oxidation of PAR as well as larger faradic currents was achieved at LNT–CFO/GCE, indicating that LNT–CFO nanoparticles have more favorable promotion to the oxidation of PAR. According to the literature [34], the oxidation of PAR to N-acetyl-p-benzoquinone-imine may be catalyzed by the La[Ni^{III}Ni^{II}]$_x$[Ti^{V}Ti^{III}]$_{1-x}$O$_{3-y}$ in PBS. The main product in the electrooxidation of PAR in aqueous solution containing 0.1 M PBS (pH=7.0) is dimer 1 (Scheme 1). In heterogeneous reactions that occur with electron transfer on perovskite-type oxides, the active sites are generally the transition metal ions with partially occupied d orbitals. The perovskite-type oxides LNT–CFO may be considered as catalysts with transition metals in mixed oxidation states with the formula La[Ni^{III}Ni^{II}]$_x$[Ti^{V}Ti^{III}]$_{1-x}$O$_{3-y}$ where y stands for oxygen vacancies [35]. So, from what was stated above, some of these transition ions are expected to be the active sites for the oxidation of PAR.

The influence of scan rate (ν) on the electrochemical behavior of PAR on LNT–CFO/GCE was investigated (Fig. 4). In the range of 20–380 mV/s, the redox peak current increases linearly with $\nu^{1/2}$, demonstrating the diffusion-controlled process of PAR on LNT–CFO/GCE. The linear regression equations were I_{pa} (μA)=−1.766–
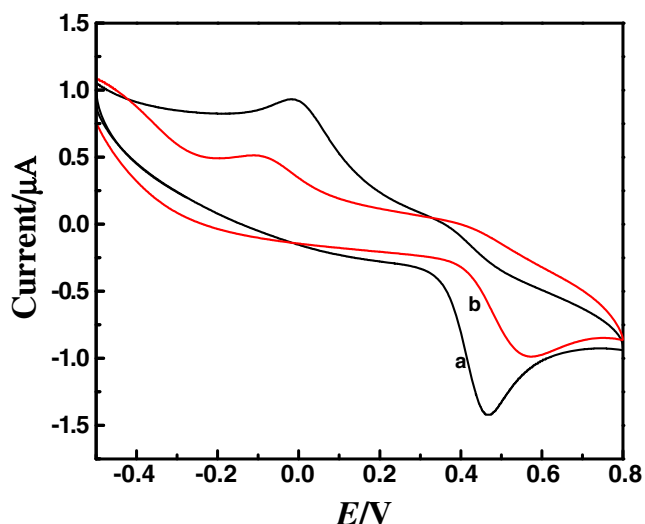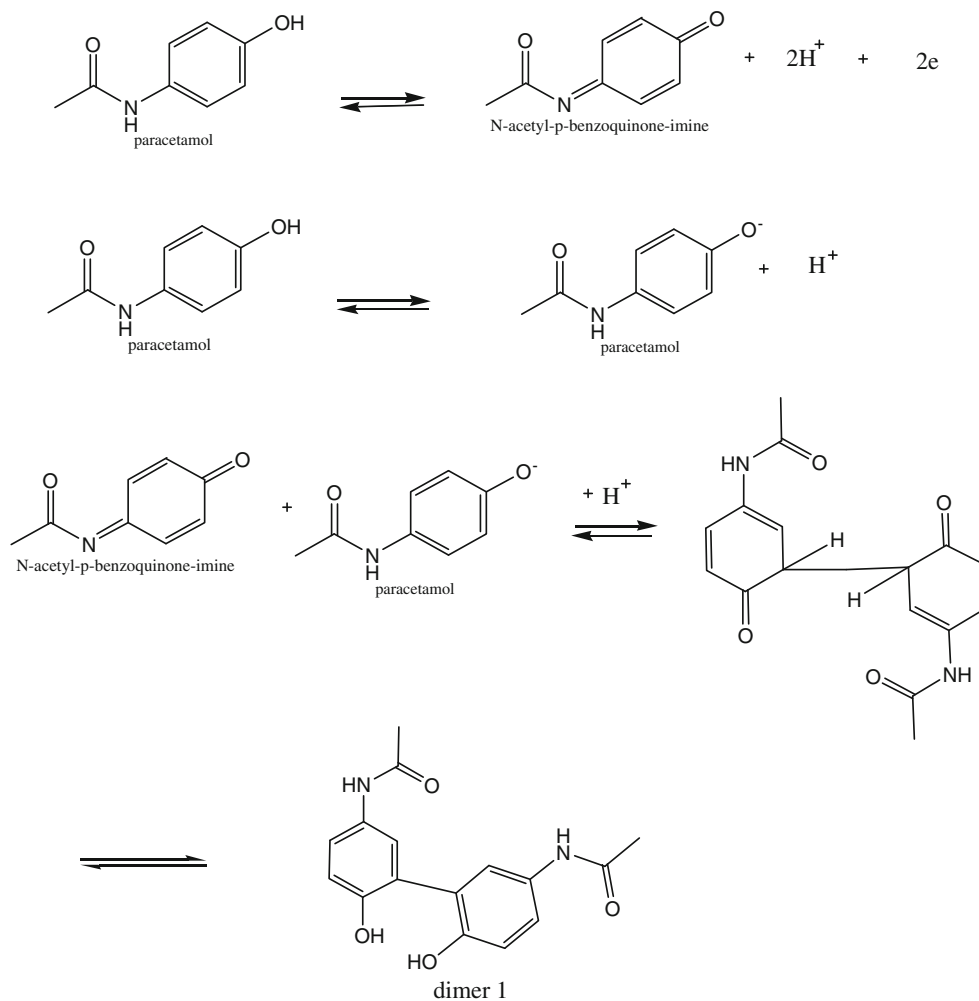
Fig. 2 **a** CV of bare GCE in 0.1 M PBS (pH 7.0); **b** CV of LNT-CFO/GCE in 0.1 M PBS (pH 7.0). Scan rate, 100 mV/s

Fig. 3 CVs of the bare GCE (*b*) and LNT–CFO/GCE (*a*) with 0.3 mM PAR in 0.1 M PBS (pH 7.0) at the scan rate of 100 mV/s

19.58 $\nu^{1/2}$ (V/s)$^{1/2}$ and I_{pc} (µA)=0.2145+7.9645 $\nu^{1/2}$ (V/s)$^{1/2}$ with correlation coefficients of 0.9963 and 0.9958.

Optimization of LNT–CFO/GCE sensor performance

The effects of pH values on PAR determination

The pH value of the solution has a significant influence on the peak potential of the catalytic oxidation of PAR. Linear sweep voltammetries (LSV) of the GCE and LNT–CFO/GCE were performed in supporting electrolyte solutions (pH 5–11) without PAR. As shown in Fig. 5a, the LSV curves had no obvious differences with various pH values. However, the pH value of the solution has a significant influence on the peak potential of the catalytic oxidation of PAR. Figure 5b illustrates the dependence of the LSV peak potential of PAR on the pH. As can be seen, the peak potential for PAR oxidation varies linearly with pH and shifts to more negative potentials with pH increasing. This behavior was attributed to an increasing amount of hydrolysis that occurs as the proton (s) is increased, leading to the formation of reducing compounds such as *p*-hydroxyaniline [36]. The equation is E_p=0.7256−0.03736pH (R=−0.998). The theoretical slope of the plot of E_{pa} versus pH for a classical Nernstian two-

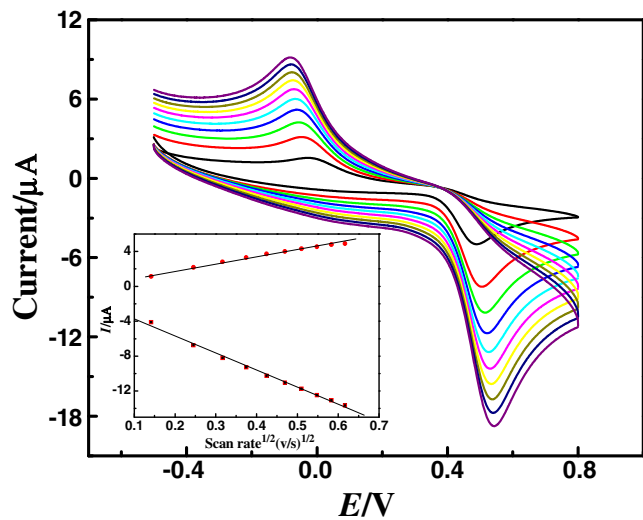**Scheme 1** The reaction mechanism of electrooxidation of PAR

Fig. 4 CVs of LNT–CFO/GCE in 0.1 M PBS (pH 7.0) solutions including 0.1 mM PAR at different scan rates (20–380 mV/s). *Inset* is the linear dependence of peak current with the square root of scan rate

Fig. 6 Effect of concentration of LNT–CFO on PAR (0.2 and 0.3 mM) determination

electron, two-proton process is −59 mV pH^{-1}. A slope of −37 mV pH^{-1} obtained in these experiments indicates that the electrode process is more complex. It also can be seen that I_p reached a maximum value at pH 7.0. Therefore, pH 7.0 was chosen in the following experiments.

The effect of concentration of LNT–CFO on PAR determination

The relationship between I_p of PAR and the concentration of LNT–CFO was investigated by LSV (Fig. 6). The I_p of 0.2 and 0.3 mM PAR was determined in 0.1 M PBS (pH 7.0). The I_p increased with increasing concentrations of LNT–CFO between 0 and 1 mg/mL and then decreased
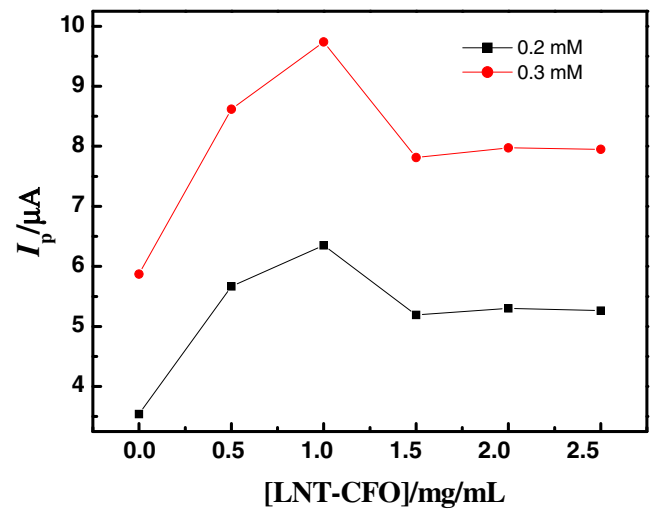
above 1 mg/mL, which may be ascribed to the thicker film of the electrode surface which hampers electron transfer. The concentration of LNT–CFO suspension was kept at 1 mg/mL in further experiments.

The effect of applied potentials on PAR determination

The influence of applied potentials on the I_p of PAR oxidation was performed in 0.1 M PBS (pH 7.0) in the range of +0.4 to +0.6 V (Fig. 7). It is obvious that the I_p increased rapidly with the increase of applied potential when the potential was lower than +0.5 V. When the potential was higher than +0.5 V, I_p almost attained a plateau. The response (below 0.5 V) increased due to the increasing deriving force for the electro-oxidation of PAR
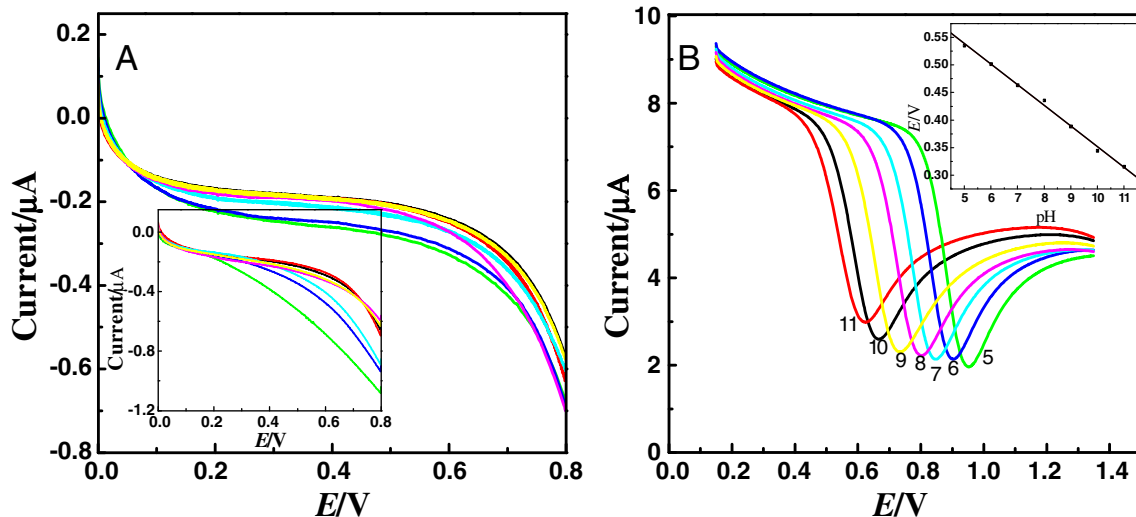

Fig. 5 **a** LSV of LNT–CFO/GCE in 0.1 M PBS at different pH values (5–11). *Inset*, LSV of GCE in 0.1 M PBS at different pH values. **b** LSV of LNT–CFO/GCE in 0.1 M PBS with 0.2 mM PAR at different pH values (5–11). *Inset*, plots of E_p vs. pH. Scan rate, 100 mV/s
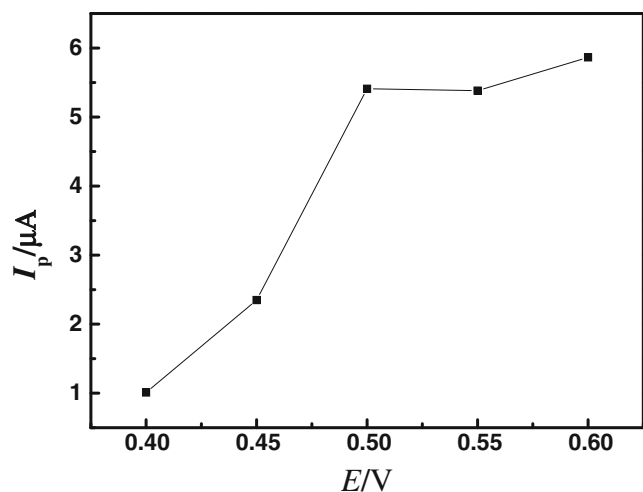
Fig. 7 The influence of applied potentials on the I_p of PAR oxidation performed in 0.1 M PBS (pH=7.0) in the range of +0.4 to +0.6 V

[37]. Over 0.5 V, the response of the sensor was controlled by diffusion of the substrate and product [38]. So, the applied potential of +0.5 V was chosen in the following experiments.

Calibration curve and interferences

Figure 8 shows the successive addition of PAR into 0.1 M PBS (pH=7.0) at the potential of 0.5 V. The rapid amperometric response on LNT–CFO film is proportional to the respective analyte concentration. A linear response in concentration range is from 0.5 to 901 μM. The linear regression equation is expressed as I_p (μA)=−0.40197−0.01793 C (μM) with a correlation coefficient of 0.9998.
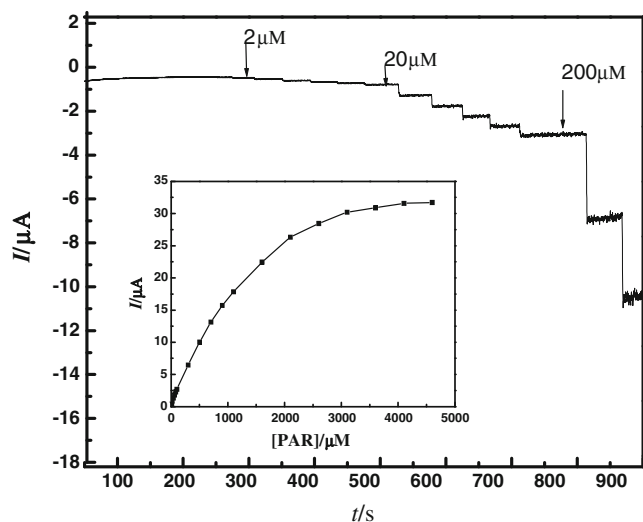

Fig. 8 Current–time curves obtained at LNT–CFO/GCE upon successive addition of different concentrations of PAR into 0.1 M PBS (pH 7) with applied potential at 0.5 V. *Inset* is the calibration curve for PAR at LNT–CFO/GCE

Table 1 Comparisons of the performance of the proposed sensor with the reported one

Modified electrode	Linear working range (μM)	Detection limit (μM)	reproducibility	References
C–Ni/GCE	7.8–110	0.6	1.1% (n=12)	[30]
Graphene/GCE	0.1–20	0.032	5.2% (n=6)	[31]
FeTPyPz/GCE	4.0–420	1.2	3.4% (n=7)	[39]
FeTPyPz/GCE	10–50,000	1.0	1.2% (n=7)	[40]
Nano-Au/PG/CPE	0.05–70	0.01	2.9% (n=10)	[41]
LNT–CFO/GCE	0.5–901	0.19	1.7 % (n=6)	This work

C–Ni/GCE carbon-coated nickel magnetic nanoparticles-modified glassy carbon electrodes, *FeTPyPz/GCE* iron tetrapyridinoporphyrazine-modified glassy carbon electrodes, *Nano-Au/PG/CPE* nanosized gold particles and poly glutamic acid-modified carbon paste electrode

The determination limit of PAR is 0.19 μM. A comparison of the response characteristics for different modified electrodes is shown in Table 1.

The effects of common interfering species on the biosensor response were examined. The interference experiments were performed in 0.1 M PBS (pH 7.0) under optimal conditions by comparing the response current of 5 μM PAR plus each interfering substance with that of 5 μM PAR alone. The results obtained are listed in Table 2. As shown in Table 2, various common salts such as KCl, MgSO$_4$, ZnSO$_4$, CH$_3$COONa, InSO$_4$, PbSO$_4$, and some small molecules such as glucose and citric acid hardly interfered. A total of 1,000 times of CuSO$_4$ and CdSO$_4$ interfered slightly, probably owing to their catalytic oxidation of PAR. This effect was even more pronounced

Table 2 Results of the interfering experiment

Interferent	Concentration (mM)	Current ratio[a]
CdSO$_4$	5	0.849
NiCl$_2$	5	0.679
InSO4	5	0.998
CuSO$_4$	5	0.839
MgSO$_4$	5	0.987
ZnSO$_4$	5	0.988
PbSO$_4$	5	0.969
KCl	5	1
CH$_3$COONa	5	1
Glucose	5	0.978
Citric acid	5	0.957

[a] Ratio of currents for mixtures of interferents and 5 μM PAR compared to that for 5 μM PAR alone. Applied potential, 0.5 V. Electrolyte, 0.1 M PBS (pH 7.0)

for 1,000 times of NiCl$_2$, which can be attributed to its stronger promotion to PAR.

Reproducibility and stability of the biosensor

The reproducibility of LNT–CFO-modified GCE was studied by repeating the determination of 0.3 mM PAR. After each determination, the modified electrode used underwent ten successive CV sweeps between −0.8 and 0.5 V at the rate of 100 mV/s in the PBS (pH 7) to remove any adsorbents and is regenerated. The six measurements achieved good reproducibility with the RSD of 1.7%.

The electrochemical stability of LNT–CFO/GCE was checked by continuous cyclic scanning at the scan rate of 100 mV/s. The result shows that the peak currents maintained about 97% of its original intensity after 60 cycles, indicating that the biosensor possesses good stability. Moreover, the biosensor remained 92.6% of its initial response after 1 month of storage. The good reproducibility and stability can be ascribed to the unique structure of LNT–CFO.

Analysis of commercial samples

The practical application of the present method was demonstrated by determining the concentration of the commercial drugs (Fen An ka Min Pill). The tablets were ground to powder and dissolved in double-distilled water, and then the suspension was filtered. Using the proposed method, the concentration of PAR of the pharmaceutical preparation was detected (143.7 mg/tablet), which is in good agreement with the concentration of PAR provided by the manufacturer (150 mg). The recovery tests of adding PAR were performed using a current–time curve. The average recovery of the tests was 95.8%. The result indicates that the sensor developed in this work has high sensitivity for detecting PAR in commercial tablets.

Conclusions

A novel sensor based on LNT–CFO-modified GCE was developed. It shows the advantages of relatively easy fabrication, high reproducibility, and sufficient long-term stability. Further, it has been found that LNT–CFO film has excellent promotion to the oxidation of PAR. In the meantime, the sensor exhibits fast amperometric response, wide linear range of concentration change, and low determination limit. The proposed method can be applied to pharmaceutical formulations with satisfactory results.

References

1. Willner I, Willner B, Katz E (2007) Biomolecule–nanoparticle hybrid systems for bioelectronic applications. Bioelectrochemistry 70:2–11
2. Zhang JD, Oyama M (2005) Gold nanoparticle-attached ITO as a biocompatible matrix for myoglobin immobilization: direct electrochemistry and catalysis to hydrogen peroxide. J Electroanal Chem 577:273–279
3. Feng WY, Xu XH, Wang H, Zhou JT, Yang XN, Zhang Y, Shang SX, Huang BB (2004) Photocatalytic property of perovskite bismuth titanate. Appl Catal B: Environ 52:109–116
4. Rached H, Rached D, Rabah M, Khenata R, Reshak A (2010) Full-potential calculation of the structural, elastic, electronic and magnetic properties of XFeO$_3$ ($X_{1/4}$Sr and Ba) perovskite. Physica B 405:3515–3519
5. Li GB, Liu SX, Liao FH, Tian SJ, Jing XP, Lin JH, Uesu Y, Kohn K, Saitoh K, Terauchi M, Di N, Cheng ZH (2004) The structural and electric properties of the perovskite system BaTiO$_3$–Ba(Fe$_{1/2}$Ta$_{1/2}$)O$_3$. J Solid State Chem 177:1695–1703
6. Liao KF, Chang YS, Chai YL, Tsai YY, Chen HL (2010) Structure and dielectric properties of sodium-doped Ba(FeNb)$_{0.5}$O$_3$. Mater Sci Eng B 172:300–304
7. Kim CY, Niihara OSK (2010) Optical, mechanical, and dielectric properties of Bi$_{1/2}$Na$_{1/2}$TiO$_3$ thin film synthesized by sol–gel method. J Sol-Gel Sci Technol 55:306–310
8. Mazaheri M, Akhavan M (2010) Electrical behavior of nano-polycrystalline (La$_{1/y}$K$_y$)$_{0.7}$Ba$_{0.3}$MnO$_3$ manganites. J Magn Magn Mater 322:3255–3261
9. Bai SL, Luo RX, Shi BJ, Liu ZY, Li DQ (2010) Gas sensing property of MgO modified LaFeO$_3$ nanocomposites. IEEE Sens J 10:1633–1634
10. Yoon KJ, Cramer CN, Stevenson JW, Marina OA (2010) Advanced ceramic interconnect material for solid oxide fuel cells: electrical and thermal properties of calcium- and nickel-doped yttrium chromites. J Power Sources 195:7587–7593
11. Ding XF, Kong X, Jiang JG, Cui C, Guo XX (2010) Characterization and V electrochemical performance of (Ba$_{0.6}$Sr$_{0.4}$)$_{1−x}$La$_x$Co$_{0.6}$Fe$_{0.4}$O$_{3−\delta}$ ($x=0$, 0.1) cathode for intermediate temperature solid oxide fuel cells. Mater Res Bull 1272:1271–1277
12. Zhao F, Wang SW, Kyle B, Chen FL (2010) Layered perovskite PrBa$_{0.5}$Sr$_{0.5}$Co$_2$O$_{5+\delta}$ as high performance cathode for solid oxide fuel cells using oxide proton-conducting electrolyte. J Power Sources 1955:468–5473
13. Ding HP, Xue XJ (2010) Novel layered perovskite GdBaCoFeO$_5$Dd as a potential cathode for proton-conducting solid oxide fuel cells international. J Hydrogen Energy 35:4311–4315
14. Ding HP, Xue XJ (2010) Cobalt-free layered perovskite GdBaFe$_2$O$_{5+x}$ as a novel cathode for intermediate temperature solid oxide fuel cells. J Power Sources 195:4718–4721
15. Smith EA, Lokuhewa IN, Misture ST, Edwards DD (2010) p-type thermoelectric properties of the oxygen-deficient perovskite Ca$_2$Fe$_2$O$_5$ in the brown millerite structure. J Solid State Chem 183:1670–1677
16. Wang Y, Sui Y, Wang XJ, Su WH, Cao WW, Liu XY (2010) Thermoelectric response driven by spin-state transition in

La$_{1-x}$Ce$_x$CoO$_3$ perovskites. ACS Appl mater interfaces 8:2213–2217

17. Chen XH, Hu JQ, Chen ZW, Feng XM, Li AQ (2009) Nanoplated bismuth titanate sub-microspheres for protein immobilization and their corresponding direct electrochemistry and electrocatalysis. Biosens Bioelectron 24:3448–3454

18. Wang GL, Bao YY, Tian YM, Xia J, Cao DX (2010) Electrocatalytic activity of perovskite La$_{1-x}$Sr$_x$MnO$_3$ towards hydrogen peroxide reduction in alkaline medium. J Power Sources 195:6463–6467

19. Dam TVA, Olthuis W, Bergveld P (2004) Sensing properties of perovskite oxide La$_{0.5}$Sr$_{0.5}$CoO$_{3-\delta}$ obtained by using pulsed laser deposition. Sens Actuators B 103:165–168

20. Safavi A, Maleki N, Moradlou O (2008) A selective and sensitive method for simultaneous determination of traces of paracetamol and p-aminophenol in pharmaceuticals using carbon ionic liquid electrode. Electroanalysis 19:2158–2162

21. Goyal RN, Gupta VK, Oyama M, Bachheti N (2005) Differential pulse voltammetric determination of paracetamol at nanogold modified indium tin oxide electrode. Electrochem Commun 7:803–807

22. Kachoosangi RT, Wildgoose GG, Compton RG (2008) Sensitive adsorptive stripping voltammetric determination of paracetamol at multiwalled carbon nanotube modified basal plane pyrolytic graphite electrode. Anal Chimi Acta 618:54–60

23. Lourenc BC, Medeirosb RA, Rocha RCF, Mazoa LH, Fatibello OF (2009) Simultaneous voltammetric determination of paracetamol and caffeine in pharmaceutical formulations using a boron-doped diamond electrode. Talanta 78:748–752

24. Lohmann W, Karst U (2006) Simulation of the detoxification of paracetamol using on-line electrochemistry/liquid chromatography/mass spectrometry. Anal Bioanal Chem 386:1701–1708

25. Knochen M, Giglio J, Reis BF (2003) Flow-injection spectrophotometric determination of paracetamol in tablets and oral solutions. J Pharm Biomed Anal 33:191–197

26. Easwaramoorthy D, Yu YC, Huang HJ (2001) Chemiluminescence detection of paracetamol by a luminol-permanganate based reaction. Anal Chimi Acta 439:95–100

27. Reddy TM, Balaji K, Reddy SJ (2007) Voltammetric behavior of some fluorinated quinolone antibacterial agents and their differential pulse voltammetric determination in drug formulations and urine samples using ab-cyclodextrin-modified carbon-paste electrode. J Anal Chem 2:168–175

28. Babaei A, Afrasiabi M, Babazadeh M (2010) A glassy carbon electrode modified with multiwalled carbon nanotube/chitosan composite as a new sensor for simultaneous determination of acetaminophen and mefenamic acid in pharmaceutical preparations and biological samples. Electroanalysis 15:1743–1749

29. Li Y, Umasankar Y, Chen SM (2009) Polyaniline and poly(flavin adenine dinucleotide) doped multi-walled carbon nanotubes for p-acetamidophenol sensor. Talanta 79:486–492

30. Wang SF, Xie F, Hu RF (2007) Carbon-coated nickel magnetic nanoparticles modified electrodes as a sensor for determination of acetaminophen. Sens Actuators B 123:495–500

31. Kang XH, Wang J, Wu H, Liu J, Aksay IA, Lin YH (2010) A graphene-based electrochemical sensor for sensitive detection of paracetamol. Talanta 81:754–759

32. Li F, Liu JJ, Evans DG, Duan X (2004) Stoichiometric synthesis of pure MFe$_2$O$_4$ (M=Mg, Co, and Ni) spinel ferrites from tailored layered double hydroxide (hydrotalcite-like) precursors. Chem Mater 16:1597–1602

33. Wang YL, Xu YH, Luo LQ, Ding YP, Liu XJ (2010) Preparation of perovskite-type composite oxide LaNi$_{0.5}$Ti$_{0.5}$O$_3$–NiFe$_2$O$_4$ and its application in glucose biosensor. J Electroanal Chem 642:35–40

34. Nematollahi D, Shayani-Jama H, Alimoradi M, Niroomand S (2009) Electrochemical oxidation of acetaminophen in aqueous solutions: kinetic evaluation of hydrolysis, hydroxylation and dimerization processes. Electrochimi Acta 54:7407–7415

35. Falcon H, Carbonio RE, Fierro JLG (2001) Correlation of oxidation states in LaFe$_x$Ni$_{1-x}$O$_{3+\delta}$ oxides with catalytic activity for H$_2$O$_2$ decomposition. J Catalysis 203:264–272

36. Fabiana SF, Christopher MA, Brett LA (2007) Carbon film resistor electrode for amperometric determination of acetaminophen in pharmaceutical formulations. J Pharm Biomed Anal 43:1622–1627

37. Liu XJ, Luo LQ, Ding YP, Xu YH (2011) Amperometric biosensors based on alumina nanoparticles–chitosan–horseradish peroxidase nanobiocomposites for the determination of phenolic compounds. Analyst 136:696–701

38. Shan D, Wang SX, He YY, Xue HG (2008) Amperometric glucose biosensor based on in situ electropolymerized polyaniline/poly(acrylonitrile-co-acrylic acid) composite film. Mater Sci Eng C 28:213–217

39. Maria DPTS, Anderson S, Marcos RVL, Auro AT, Lauro TK (2008) Construction and application of an electrochemical sensor for paracetamol determination based on iron tetrapyridinoporphyrazine as a biomimetic catalyst of P450 enzyme. J Braz Chem Soc 19:734–743

40. Mariana CQO, Marcos RVL, Auro AT, Maria DPTS (2010) Flow injection analysis of paracetamol using a biomimetic sensor as a sensitive and selective amperometric detector. Anal Methods 2:507–512

41. Zhang Y, Luo LQ, Ding YP, Liu X, Qian ZY (2010) A highly sensitive method for determination of paracetamol by adsorptive stripping voltammetry using a carbon paste electrode modified with nanogold and glutamic acid. Microchim Acta 171:133–138